2014

Coherent Sea Level Variability on the North Atlantic Western Boundary

P. R. Thompson
University of South Florida

G. T. Mitchum
University of South Florida, mitchum@usf.edu

AGU PUBLICATIONS

JGR

Journal of Geophysical Research: Oceans

RESEARCH ARTICLE

10.1002/2014JC009999

Key Points:
- Decadal variability of western North Atlantic sea level is highly coherent
- Large-scale vertical divergence accounts for the coherent sea level fluctuations
- Vertical divergence results from net zonal transport into the boundary region

Correspondence to:
P. R. Thompson,
philiprt@hawaii.edu

Citation:
Thompson, P. R., and G. T. Mitchum (2014), Coherent sea level variability on the North Atlantic western boundary, *J. Geophys. Res. Oceans*, *119*, 5676–5689, doi:10.1002/2014JC009999.

Received 26 MAR 2014
Accepted 22 JUL 2014
Accepted article online 25 JUL 2014
Published online 3 SEP 2014

Coherent sea level variability on the North Atlantic western boundary

P. R. Thompson[1,2] and G. T. Mitchum[1]

[1]College of Marine Science, University of South Florida, St. Petersburg, Florida, USA, [2]Department of Oceanography, University of Hawai'i at Mānoa, Honolulu, Hawai, USA

Abstract Interannual to decadal sea level variability on the North Atlantic western boundary is surprisingly coherent over substantial distances stretching from the Caribbean to Nova Scotia. The physical mechanisms responsible for this basin-scale, low-frequency coherence are explored in a diagnosis of simulated ocean fields from GECCO, which reproduces the observations to good approximation. Coastal sea level variability on the western boundary is known to be influenced by meridional divergence in the boundary current resulting in a geostrophic tilting of the sea surface. This mechanism is found to be of leading order along some stretches of the boundary, but it does not account for the coherence spanning the western North Atlantic. Instead, the coherence along the entire boundary is accounted for by vertical divergence resulting in the uniform rise and fall of the sea surface west of the 295°E meridian. The vertical divergence is found to be due to net vertically integrated zonal transport across this meridian resulting from meridional variation in the Sverdrup transport over the basin interior.

1. Introduction

Sea level change is an important indicator of climate and oceanographic variability on a variety of time and spatial scales [e.g., *White et al*., 2008]. Much attention is given to the global rate of change, but regional rates can be an order of magnitude larger than the global value [*Cazenave and Nerem*, 2004]. Understanding large-amplitude regional sea level change is important for coastal planning, studies of ocean and climate dynamics, and reducing the error bar about estimates of the global rate. The North Atlantic is of particular interest due to the concentration of coastal urban populations and the role of the Gulf Stream in global climate. There are many proposed modes and mechanisms of decadal variability in the North Atlantic [e.g., *Häkkinen*, 2000; *Eden and Jung*, 2001; *Curry and McCartney*, 2001; *Wu and Liu*, 2005], and a good way to evaluate the merits of these various modes is to assess their ability to account for observed sea level variability [*Häkkinen*, 2001].

A prominent feature of coastal sea level variability in the North Atlantic is the low-frequency coherence over large spatial scales (>1000 km) on the western boundary of the basin. *Thompson* [1986] noticed that 20–25 year records of sea level along the Atlantic North American coast could be classified based on large-scale coherence into two groups—those north of the Gulf Stream separation and those south of the separation. *Maul and Hanson* [1991] documented large-scale coherence stretching from the Southeast U.S. (SE) into the Gulf of Mexico (GOM) from the 1930s to 1980s, and *Douglas* [2005] later showed from a few limited records that Caribbean sea level is also coherent with the GOM and SE regions. In contrast to *Thompson* [1986], *Häkkinen* [2000] noted that at decadal timescales, the gauges in the Northeast U.S. (NE) are positively correlated with gauges in the SE. All of these results are noteworthy, because they demonstrate that coherence in western North Atlantic sea level spans oceanographic boundaries, such as the Gulf Stream separation, and geographic boundaries, such as the Straits of Florida.

Low-frequency sea level variations in the North Atlantic are correlated with variations in the intensity and location of atmospheric pressure centers [*Maul and Hanson*, 1991; *Woolf et al*., 2003; *Kolker and Hameed*, 2007; *Miller and Douglas*, 2007], but the inverted barometer effect does not explain the relationship [e.g., *Maul and Hanson*, 1991; *Miller and Douglas*, 2007]. The atmosphere and coastal sea level are thus dynamically linked, but it remains unclear what mechanisms are responsible for the basin-scale coherence. Gulf Stream transport variability is a mechanism with the potential to homogenize sea level variations over

extended stretches of coastline. Sea level differences across the North Atlantic western boundary current are related to variations in geostrophic transport [*Montgomery*, 1938, 1941; *Wunsch et al*., 1969; *Maul et al*., 1985]. Relating the transport changes to wind-stress, however, can be difficult. For example, *Thompson* [1986] found no link to Sverdrup transport from calculations of wind-stress-curl (WSC) in relatively short (20–25 years) records of coastal sea level along the Gulf Stream. This may be because the Sverdrup balance requires time for the gyre circulation and wind forcing to equilibrate.

Hong et al. [2000] avoided the equilibration time scale by employing the time-dependent, quasigeostrophic Rossby wave model of *Sturges and Hong* [1995] to relate coastal sea level on the western boundary to open ocean WSC. The Rossby wave model provides estimates of zonal transport anomalies into the western boundary region, which can be assumed to accelerate or decelerate the boundary current resulting in changes in the geostrophic tilt of the ocean surface. This model was able to account for significant fractions of coastal sea level variability at periods longer than 5 years from Fernandina, Florida, and Lewes, Deleware [*Hong et al*., 2000]. Recently, this mechanism has been associated with a localized "hotspot" of sea level rise in recent decades north of the Gulf Stream separation [*Sallenger et al*., 2012; *Ezer et al*., 2013]. The focus of this work, however, is coherent variability of larger spatial scale over an earlier and longer period.

Häkkinen [2001] analyzed hind-cast simulations of the North Atlantic and found the leading modes of gyre circulation and western Atlantic SSH variability to be primarily due to thermal forcing and meridional overturning. In particular, western boundary SSH variations were found to reflect changes in upper ocean heat content, which differs from the geostrophic tilting mechanism of *Hong et al*. [2000]. *Bingham and Hughes* [2009] related coherent sea level along the Northeast U.S. coast in altimetry and tide gauges to meridional overturning, which is consistent with the findings of *Häkkinen* [2001]. Other processes, such as alongshore winds and river runoff, are possible drivers of coastal sea level change, but these were found to be unimportant at low frequencies in the North Atlantic western boundary [*Hong et al*., 2000].

The works cited above account for large-scale sea level variability in portions of the North Atlantic western boundary region via a variety of mechanisms. We will show, however, that a majority of the low-frequency coastal sea level variability since 1950 is coherent across the entire western boundary from the Caribbean to Nova Scotia. Thus, the mechanism responsible for the basin-scale coherence over this period is not likely to be geostrophic tilting of the surface, which would tend to result in coastal anomalies of opposite sign across the Gulf Stream separation. In the following analysis, we demonstrate the large-scale coherence and isolate the coherent fraction of the observed variability from tide gauges. We then diagnose output from an ocean model capable of reproducing the coherent sea level fluctuations in order to assess the physical mechanisms responsible for the large-scale, low-frequency coherence.

2. Tide Gauge Data

Monthly mean tide gauge sea levels were obtained from the Permanent Service for Mean Sea Level (PSMSL). The number of tide gauge records available along the East Coast of the U.S. is large compared to other regions of the global ocean, but in order to avoid oversampling particular stretches of coastline, preference was given to long records beginning before 1950. In cases where multiple long records were available in close proximity, time series with the fewest gaps were given priority, and gauges located in bays or estuaries were rejected in favor of gauges at open ocean boundaries. The number and quality of tide gauge records decreases substantially along non-U.S. coastlines, but the coherence of sea level is known to extend to the Caribbean as shown by *Douglas* [2005], who showed low-frequency sea level variations at Pensacola were similar and in phase with sea level in Cuba and Puerto Rico. This similarity is not expected from the results of *Hong et al*. [2000], because the eastern Caribbean would appear to be offshore of the Gulf Stream and should vary out of phase with Pensacola [*Douglas*, 2005]. Few quality tide gauge records are available in the Caribbean Sea (CS), but three Caribbean gauges were deemed long enough and complete enough to contribute to the analysis. The locations of all tide gauge records used in the analysis are shown by circles in Figure 1, and information concerning the span and completeness of each series is presented in Table 1.

A monthly climatology was removed from each sea level time series in the analysis, and a trend was removed at each location over a common period (1950–2010). In addition, a quadratic trend was removed at Port Isabel, Galveston, and Grande Isle due to apparent land motion. The inverted barometer effect was

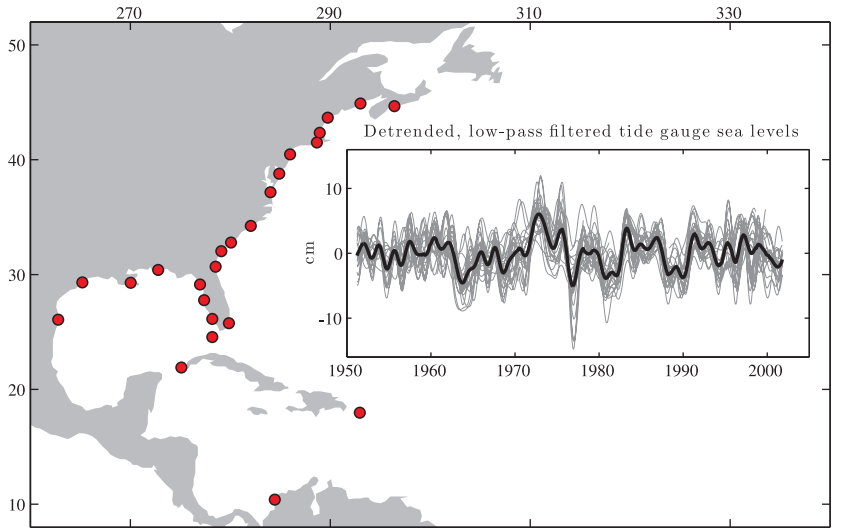

Figure 1. Tide gauge locations (red circles) and the detrended, low-pass filtered sea level time series (gray lines) used in the analysis. The thick black line is the average of the individual time series and accounts for greater than 50% of the variance in the low-passed data set.

removed using the closest sea level pressure time series to each gauge from the NCEP/NCAR 2.5° ×2.5° Reanalysis [*Kalnay et al*., 1996].

After removing the monthly climatology, substantial variability remained at periods just longer than a year. Spectral analysis revealed a peak in energy at around 14 months that is associated with a known pole tide in sea level [e.g., *Miller and Wunsch*, 1973] due to variability in the orientation of Earth's rotation axis known as the Chandler Wobble [*Chandler*, 1891]. If not handled properly, the energy at 14 months could leak into lower frequencies during the filtering process. We calculated the equilibrium pole tide at each tide gauge location from earth orientation parameters obtained from the website of the International Earth Rotation and Reference System Service (IERS) [*Vondrak et al*., 1995]. We subtracted the pole-tide variability from the tide gauge series, which effectively removed the spectral peak.

Table 1. Tide Gauges Listed by Region[a]

Region	Location	Span (since 1950)	Missing (%)
GOM	Port Isabel, TX	1950–2009	4.72
	Galveston, TX	1950–2009	0.98
	Grande Isle, LA	1950–2009	5.42
	Pensacola, FL	1950–2009	1.67
	Cedar Key, FL	1950–2009	6.25
	St. Petersburg, FL	1950–2009	0.00
	Naples, FL	1965–2009	3.72
	Key West, FL	1950–2009	1.25
SE	Miami Beach, FL[b]	1950–1981	10.85
	Haulover Pier, FL[b]	1987–1992	4.41
	Virginia Key, FL[b]	1994–2009	1.57
	Fernandina, FL	1950–2009	4.17
	Fort Pulaski, GA	1950–2009	1.39
	Charleston, SC	1950–2009	0.00
	Wilmington, NC	1950–2009	2.08
NE	Kiptopeke Beach, VA	1951–2009	0.71
	Lewes, DE	1950–2009	5.14
	Sandy Hook, NJ	1950–2009	1.39
	Newport, RI	1950–2009	1.53
	Boston, MA	1950–2009	1.39
	Portland, ME	1950–2009	0.42
	Eastport, ME	1950–2009	9.17
	Halifax, Nova Scotia	1950–2008	3.11
	St. John's, Newfoundland[c]	1957–2008	4.01
CS	Cabo San Antonio, Cuba	1971–2009	20.65
	Cartegena, Colombia	1950–1992	4.65
	Isla Magueyes, PR	1955–2009	4.39

[a]For each gauge, the span of monthly data since 1950 included in the study is given with the percentage of missing monthly values during the period analyzed. Not all gauges were included in the regional analysis.
[b]Merged into a single series for analysis.
[c]Excluded from analysis.

Remaining high-frequency variability was removed using a convolution low-pass filter with half-amplitude response at 18 months. The filter passed less than 10% of the amplitude at periods shorter than 1.3 years and passed greater than 90% of the amplitude at periods longer than 1.9 years. The low-passed monthly mean series (Figure 1, gray lines) visually illustrate the basin-scale covariance spanning the western North Atlantic at interannual to decadal periods.

The average of the time series from individual gauges (Figure 1, black line) accounts for 52% of the total variance

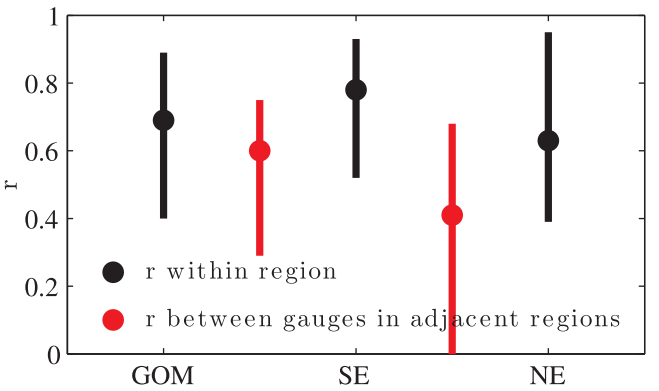

Figure 2. Median, maximum, and minimum correlations between time series within each region (black) compared to the median, maximum, and minimum correlations between time series in adjacent regions (red).

in the low-passed data set and represents the coherent portion of the sea level variability. There are intervals, particularly near the beginning and end of the analysis period, when the amplitude of the coherent signal is small and the variability is dominated by differences between the gauges. In the following analyses, we are primarily concerned with the physical mechanisms that account for the basin-scale, coherent variability, which is most apparent in the quasi-decadal fluctuations of the mean curve during 1960–1995. Unfortunately, this limits the usefulness of satellite altimetry data set (1993–present), because the ratio of the coherent signal to regional noise is too small during the satellite era.

3. Region Definitions

The first objective was to reduce the dimensionality of the tide gauge data set in order to make the diagnosis of the dynamics more tractable. We achieve the reduction of dimensionality by grouping the gauges into regions such that a maximum amount of variance is accounted for with as few curves as possible. Ideally, the set of curves would be composed of a small number of regional time series, each of which represents a large fraction of the variance in a subset of the gauges. The limited data available in the Caribbean were averaged into a single regional curve, but it was not obvious how to group the remaining tide gauges along the U.S. and Canadian coasts. The basic principle applied to defining the regions was to maximize correlation of the sea level series within each region while simultaneously minimizing the correlation between gauges in adjacent regions. A logical first guess for the regional boundaries was to make physically sensible delineations based on geographic and oceanographic features. In the western North Atlantic, two such features are the Straits of Florida and the Gulf Stream separation. Thus, we initially defined four regions in which to group the tide gauges: Caribbean Sea (CS), Gulf of Mexico (GOM), Southeast (SE), and Northeast (NE). The first two are defined by the Yucatan Strait and the Straits of Florida, and the latter two are defined to be along the U.S. Atlantic coast south and north of the Gulf Stream separation, respectively.

We tested the validity of these groupings using an agglomerative hierarchical cluster analysis, which is an objective method for grouping entities. In this case, we chose to use correlation as a basis for the clustering algorithm. The results of the cluster analysis are not detailed here, because they essentially confirmed the logic of the initial guess. The gauges at Naples, Key West, and Miami appeared to be equally well suited to cluster with either gauges in the Gulf of Mexico or gauges along the Southeast coast of the U.S. We chose to absorb the Naples and Key West gauges into the Gulf of Mexico region and the Miami gauge into the Southeast region on the basis of natural geographic boundaries. We also chose to exclude the gauge in St. John's, Newfoundland from any region, because it did not cluster within a reasonable correlation.

The first column of Table 1 lists the region for each gauge. Figure 2 shows the median, maximum, and minimum correlations between time series within each region compared to the median, maximum, and minimum correlations between time series in adjacent regions. The low correlation between gauges from adjacent regions compared to relatively higher correlations within regions supports the region definitions. Figure 3 shows the regional time series calculated as the mean at each time over the gauges in each region. Together, the regional series account for 79% of the total variance in the tide gauge data set. The mean of the regional curves, shown in black, captures the bulk of this variance (52% of the total) and represents the basin-scale variability we seek to understand.

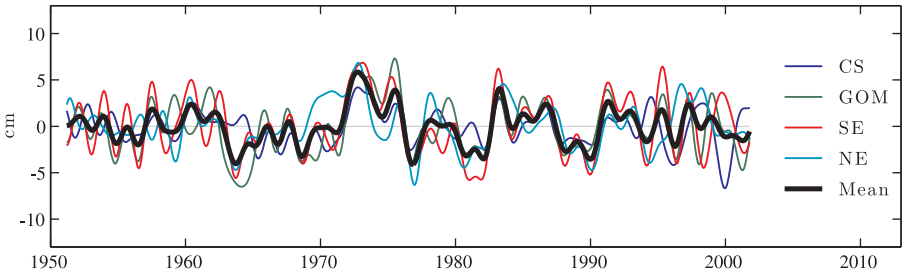

Figure 3. Regional tide gauge sea level time series. The mean of the regional series is shown as the thick black line.

4. The GECCO Model

Averaging gauges within regions reduced the dimensionality of the tide gauge data set to four regional curves while still accounting for almost 80% of the variance at periods longer than 2 years. Mechanisms responsible for the evolution of the regional curves are ideally separated into those responsible for basin-scale coherence and those responsible for regional differences. Oceanic observations are unfortunately not available at the desired spatial and temporal scales necessary to effectively separate the effects of various processes in the tide gauge time series. A model is one way to overcome the limitations of sparse observations, but the model must be able to reproduce the observed coastal sea level. A model capable of reproducing the coherent tide gauge observations provides a dynamically consistent framework in which to diagnose the processes likely to have produced the observations. The important processes in the model are not guaranteed to represent nature, but they do represent at least one feasible physical explanation.

4.1. Model Description

The model we chose is the German contribution to the consortium for Estimating the Circulation and Climate of the Ocean [GECCO, *Köhl et al*., 2006], which is an effort to assimilate in situ and satellite data using the ECCO/MIT joint ocean circulation model [*Marshall et al*., 1997a, b] over the 50 year period from 1952–2001. The model is configured with $1^{\circ} \times 1^{\circ}$ horizontal resolution between latitudes 80°S and 80°N with 23 vertical layers. The governing equations are hydrostatic with an implicit free surface, meaning sea surface height (SSH) is not an explicit variable but rather computed a posteriori from the model solution. The model is forced by 12 hourly horizontal wind-stress and daily surface fluxes derived from NCEP Reanalysis, and the optimization of the solution toward the assimilated observations was performed via the adjoint method. The computed oceanic model fields and atmospheric forcing are available as monthly means on the computational grid and were obtained from the ECCO website (http://www.ecco-group.org). The available fields are velocity (u, v, w), potential temperature (T_{θ}), salinity (S), sea surface height (η), atmospheric wind-stress, and surface fluxes of salt and heat.

We note that GECCO assimilates tide gauge data, which initially raised questions about the validity of using GECCO to assess the important physics associated with the observations. We were concerned by the potential for coastal SSH in GECCO to be forced toward the observations in an unphysical manner. However, we do not find the assimilation of the tide gauge data to be problematic. The weights given to the tide gauge observations were small and the misfits of the solution to the observations were unchanged during the optimization [*Köhl and Stammer*, 2008]. Thus, the evolution of the model solution can be assumed to be largely independent of the assimilated tide gauge observations. In addition, we tested this assumption by examining the model output in areas surrounding open ocean island gauges at Bermuda and Midway Island. In the case where assimilated tide gauge data affected the solution in a dynamically inconsistent manner, we expected to find a region of influence around each tide gauge where the solution differed with grid cells further from the gauge. No evidence for unphysical forcing of the solution toward the tide gauge sea levels during the assimilation was found in our tests of the GECCO output.

4.2. Comparison of Model to Observations

Observations from individual tide gauges were first compared with corresponding time series from the nearest GECCO grid points (not shown). Correlations were highly significant, providing confidence in the ability of GECCO to reproduce the observations. For our purposes, however, we needed to create regional

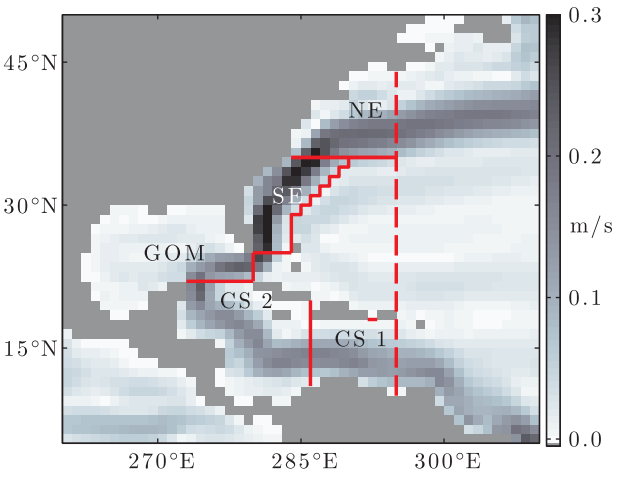

Figure 4. Boundaries of the regions defined in the GECCO domain (solid red lines). The 295°E meridian (dashed red line) intersects both North and South America and creates a closed volume to the west. Shading represents average upper 100 m surface velocity in GECCO and illustrates the average position of the western boundary current in the model.

series from GECCO analogous to the regional averages of the tide gauge series. We also needed to define two-dimensional subdomains near each coastal region in which to diagnose the important physics for coastal sea level variability. The locations of regional boundaries in the GECCO grid are based on the same geographic and oceanographic boundaries that proved useful when grouping the tide gauges. The boundaries are shown as red lines in Figure 4. Model regions were defined for the GOM, SE, and NE. The Caribbean Sea was split into two regions (CS1 and CS2) for the diagnosis due to the size of the Caribbean Sea and because the boundary current changes orientation between the two regions.

Regional time series of coastal SSH from GECCO were calculated as the average over all coastal grid points in each region during each month. The mean annual cycle was removed and each series was low-pass filtered identically to the observations. A quadratic trend was removed from each model series due to apparent drifts in the model solution, which is distinct from the linear trends we removed from the tide gauge series that result primarily from land motion.

The observed regional sea level curves are shown with the low-passed and filtered regional series from the model in Figure 5. Correlations are greater than 0.7 and significance levels from Monte Carlo simulations exceed 95% in the GOM, SE, and NE regions. The lower correlation in the CS region is likely due to the limited available tide gauge data. The mean over the observed regional series and the mean over the regional series from GECCO are the bottom pair of curves. The correlation between the two mean series is 0.78. Therefore, the model reproduces the observed regional sea level variability to good approximation. In particular, the regional curves from GECCO contain a component that is coherent over all regions, and the coherent variability is significantly correlated to the observed basin-scale variation from tide gauges.

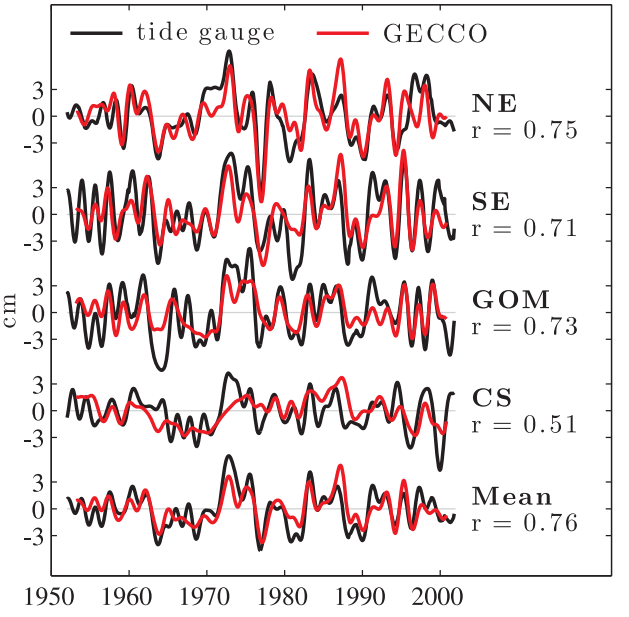

Figure 5. Regional tide gauge series (black) and average GECCO SSH from coastal grid cells in each region (red).

5. Model Diagnosis

We established in section 4 that GECCO is able to reproduce the coherent basin-scale coastal height variability observed by tide gauges, which allows us to diagnose the model fields and

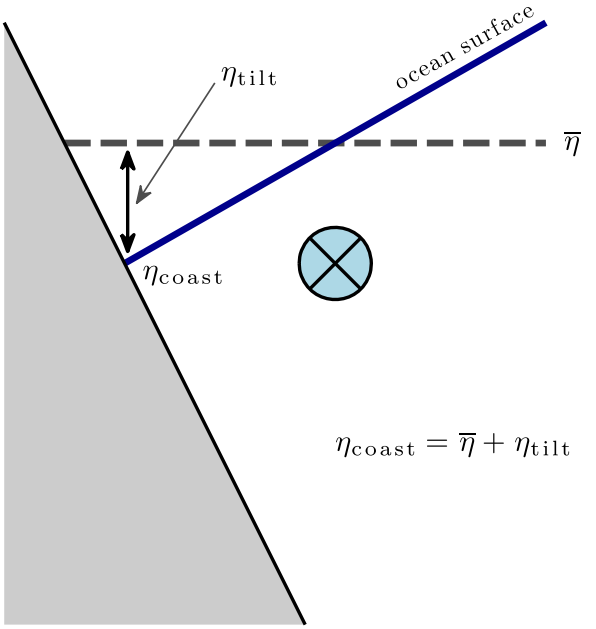

Figure 6. Schematic representation of the equation used to diagnose the GECCO model output.

assess the physical mechanisms resulting in the basin-scale coherence. We first derive a simple diagnostic equation for coastal height and then calculate the terms in the diagnostic from the model fields. Finally, we relate the coherent basin-scale variability to the large-scale wind field over the North Atlantic.

5.1. Diagnostic Equation

The diagnostic equation is formed from continuity and cross-shore geostrophic balance, which in terms of sea surface height (η) can be written

$$\frac{\partial \eta}{\partial t} = -\nabla_H \cdot \mathbf{U}, \tag{1}$$

$$\frac{\partial \eta}{\partial x} = \frac{f}{g} v_s, \tag{2}$$

where ∇_H is the horizontal gradient operator, $\mathbf{U}$ is the vertically integrated horizontal velocity vector, x is the coordinate perpendicular to the coast, f is the Coriolis parameter, g is the gravitational acceleration constant, and v_s is the alongshore surface velocity. It is unnecessary to include the alongshore pressure gradient, because it is small in the vicinity of the western boundary current.

One way to interpret these equations is to consider what happens to the ocean surface in the case of zonal transport anomalies from the east into some region of the western boundary, such as those considered by *Hong et al*. [2000]. Due to the solid western boundary, a zonal transport into the region from the east results in convergence in the zonal direction. Since volume must be conserved, the zonal convergence must be balanced by some combination of meridional and vertical divergence. Meridional divergence is achieved by accelerating the boundary current in the region resulting in a change in the slope of the surface via (2). The divergence of horizontal flow implies that the slope across the boundary current increases at the northern boundary of the region while the slope at the southern boundary remains the same. This would result in an increase of the average slope over the region. Alternatively, if there is net transport into the region, i.e., if the meridional and zonal divergences are not equal and opposite, then the remainder will manifest as a change in the average surface height in the region via the left hand side of (1). The effects on coastal sea level from meridional divergence (η_{tilt}) and vertical divergence ($\bar{\eta}$) are illustrated in Figure 6.

It is tempting to ignore the time rate of change of the surface height on the left hand side of (1), because the magnitude of $\partial\eta/\partial t$ is small compared to transports in the region of the western boundary. This is the approach taken by *Hong et al*. [2000], and as a result only tilting of the surface is considered in their analysis. Such a scaling is only valid, however, if the rate of change in the observations is much larger than the expected rate of change in the surface height from horizontal divergence. Estimations of $\partial\eta/\partial t$ in the western boundary region from GECCO velocity fields do not support this scaling, as the estimated rates of change from GECCO are of the same order as observed rates from tide gauges. Retaining the left hand side of (1) is important in the following analyses and is essential for explaining the basin-scale coherence of sea level on the western boundary of the North Atlantic.

Integrating (1) in time for some coastal region gives an equation for the average sea surface height in that region,

$$\bar{\eta}(t) = -\frac{1}{A}\int_{t_0}^{t} U_{\mathrm{net}}\, dt, \tag{3}$$

where $\eta(t_0)=0$, A is the surface area of the region,

$$U_{\text{net}} \equiv \oint_P \mathbf{U} \cdot \hat{\mathbf{n}} dP \tag{4}$$

is the net vertically integrated transport out of the region, $\hat{\mathbf{n}}$ is the outward normal, and P is the horizontal perimeter of the region. A new variable, η', can then be defined as the surface height anomaly in a region relative to $\bar{\eta}$,

$$\eta' \equiv \eta - \bar{\eta}. \tag{5}$$

Substituting (5) into (2) and integrating from the coast (x_c) to the offshore boundary of the region (x_o) gives

$$\eta'_o - \eta'_c = \frac{f}{g} V_s, \tag{6}$$

where $V_s = \int_{x_c}^{x_o} v_s \, dx$, and η'_o and η'_c are sea surface height anomalies at the offshore and coastal boundaries, respectively. The coastal boundary (x_c) is the stretch of coastline in each region along the mainland North and South American continents (Figure 4). The offshore boundary (x_o) is either the open ocean boundary (red line) or island coastline to the right of the western boundary current flow direction. Equation (6) is parametric in the alongshore coordinate, thus average coastal sea level in a region can be calculated by averaging (6) in the alongshore direction. Using the definition of η' given in (5) and solving for coastal sea level averaged in the alongshore direction over a region gives

$$\langle \eta_c \rangle = \bar{\eta} + \left[\langle \eta_o \rangle - \bar{\eta} - \frac{\langle fV_s \rangle}{g} \right], \tag{7}$$

where $\langle\rangle$ denotes an alongshore average over the region. For simplicity, we will drop the bracket notation going forward and refer to the left hand side of (7) as η_{coast}. The first term on the right hand side, $\bar{\eta}$, represents the contribution to coastal sea level variability from a net volume increase (vertical divergence). The terms in square brackets represent variability associated with geostrophic tilting of the ocean surface about the mean (meridional divergence) and will be referred to collectively in the text and figures as η_{tilt}. The diagnostic equation with the simplified notation is illustrated in Figure 6, and in the following analysis we diagnose the relative roles of the $\bar{\eta}$ and η_{tilt} terms in each region for the basin-scale sea level coherence.

5.2. Application of the Diagnostic in GECCO

Time series of $\bar{\eta}$ for each of the defined regions in GECCO were calculated in practice as simply the average SSH over the surface grid cells in each region. However, $\bar{\eta}$ is interpreted per (3) as the time integral of the net horizontal volume transport into the regions. The interpretation is supported by Figure 7, which shows the average SSH and time integral of net horizontal volume transport into each GECCO region. Correlations are high and highly significant with the exception of the NE region in which the correlation is substantially lower. The lower correlation in the NE is likely due to shallow areas of the model domain where the available monthly averages are not sufficiently accurate to integrate the continuity equation.

Because SSH in GECCO is calculated implicitly rather than explicitly, we performed some simple tests to be sure that (6) holds as formulated in terms of SSH in the western boundary current. We found that we achieved the best agreement between the slope of the SSH and velocity when we averaged the velocity over the upper five layers of the model (or 100 m). Thus, the quantity V_s in (7) is the cross-shore average of the velocity in the upper 100 m. The quantity $\langle fV_s \rangle$ is then the average of fV_s in the along-current direction where the region geometry and trajectory of the current are straightforward (CS 1, CS 2, SE). In regions with complicated current trajectories (GOM, NE), $\langle fV_s \rangle$ is the average of fV_s at the boundaries where the current flows into and out of the region. The latter method using only the in and out flow in some regions was validated using the following form of (7),

$$\langle \eta_o \rangle - \langle \eta_c \rangle = \frac{\langle fV_s \rangle}{g}. \tag{8}$$

Using only surface flow into and out of the regions reproduced $\langle \eta_o \rangle - \langle \eta_c \rangle$ equally as well as averaging along the entire length of the current in regions where both calculations were possible.

Figure 8 shows the time series of η_{coast} calculated directly from the GECCO height field and $\bar{\eta} + \eta_{\text{tilt}}$ for all five diagnostic regions. The sum of the diagnostic terms ($\bar{\eta} + \eta_{\text{tilt}}$) is shown in red, and the GECCO SSH at the

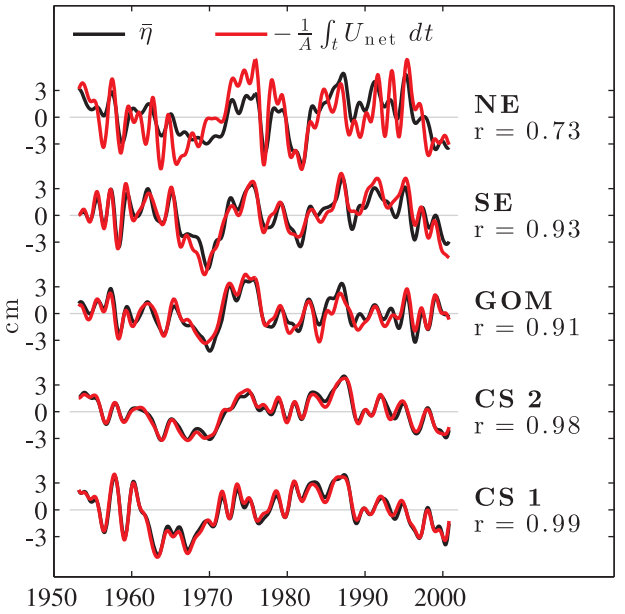

Figure 7. Average GECCO SSH in each region (black) and time-integrated net horizontal transport into each region (red). See equation (3).

coast is shown in black. Together, these curves suggest that the simplified physics included in the diagnostic are capable of reproducing the coastal SSH in the model regions to good approximation. This suggestion is supported by r^2 values between the $\eta_{\rm coast}$ and $\bar{\eta}+\eta_{\rm tilt}$ time series for each region shown in the first column of Table 2. Greater than 40% of the variance in GECCO coastal height variability is accounted for by the diagnostic in the Caribbean regions, and greater than 60% of the variance is accounted for in the GOM, SE, and NE regions. Values for r^2 are significant at the 99% level in all five regions.

The relative importance of each term in the diagnostic is also assessed, and r^2 values between the GECCO coastal height and each individual term are given in the second and third columns of Table 2. Values for r^2 are significant between $\eta_{\rm coast}$ and $\bar{\eta}$ in all five regions, but none of the r^2 values are significant between $\eta_{\rm coast}$ and $\eta_{\rm tilt}$. This suggests that net transport into each of the regions (vertical divergence) is the dominant driver of coastal height variability and not geostrophic tilting across the boundary current (meridional divergence). It is interesting to note that in the SE and NE regions, the sum of the r^2 values for the individual diagnostic terms is substantially less than the value for the sum of the terms, which indicates that the two diagnostic terms are anticorrelated. Indeed, this is true, particularly for the NE region, as shown in the last column of Table 2. It should be noted that the results of *Hong et al*. [2000] at Lewes were in what we define to be the NE region. This may explain the skill of their method despite the exclusion of vertical divergence in their formulation.

The primary objective for applying the diagnostic was to isolate the mechanism(s) responsible for the coherence between coastal sea level in each of the five regions. Figure 9a groups the $\bar{\eta}$ series from each region, and the tilting series are shown together in Figure 9b. The $\bar{\eta}$ terms from each region are visually coherent between all regions, particularly at lower frequencies, whereas the tilting terms appear to be quite different. In addition, each plot shows the average of the GECCO coastal height series over each of the five regions, which represents the sea level variability that is coherent between the regions and is denoted as $\langle\eta_{\rm coast}\rangle$. It is visually apparent from Figure 9 that the large-scale coastal sea level in GECCO is more closely related to $\bar{\eta}$ than $\eta_{\rm tilt}$, and indeed this conclusion is supported by r^2 values between the diagnostic terms from each region and $\langle\eta_{\rm coast}\rangle$ given in Table 3. The table shows that the relationship between the large-scale coherent sea level variability and the average height of the surface in each region ($\bar{\eta}$) is highly significant in all regions, whereas the relationship between the large-scale variability and the tilting term is not significant in any region. We thus conclude that the large-scale coherence of coastal sea level as reproduced by GECCO is due to vertical divergence and not accelerations of the boundary current (meridional divergence).

It was previously shown that $\bar{\eta}$ reflects the time integral of the net volume transport into each region (Figure 7), and since the $\bar{\eta}$ terms are the likely cause of coherence between regions, it is logical to inquire if basin-scale redistributions of volume into and out of the western North Atlantic are responsible for the coherent coastal variations in GECCO. Figure 10 shows $\langle\eta_{\rm coast}\rangle$ with both the average surface height west of the 295°E meridian from GECCO and the time-integrated volume transport across the 295°E meridian scaled to units of surface height. The meridian at 295°E was chosen because it intersects both North and South America creating an enclosed volume in which flow can only enter or leave across the meridian.

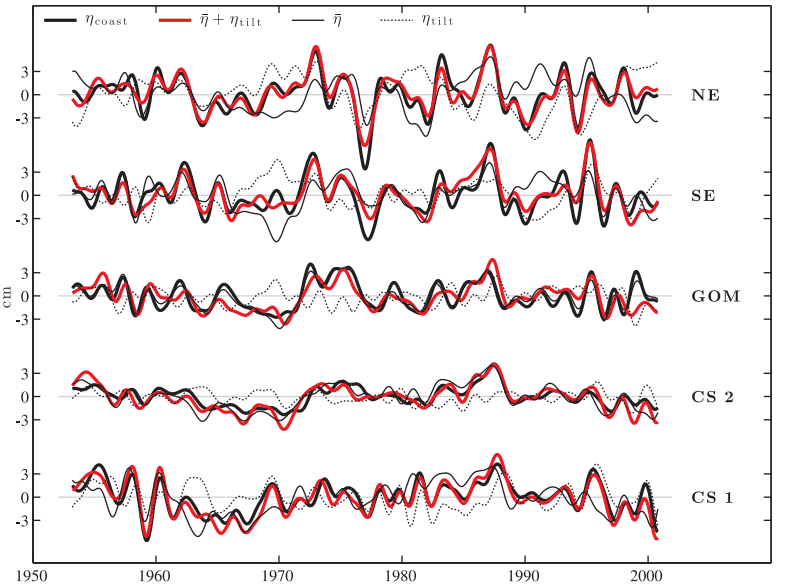

Figure 8. Diagnostic terms and their sum compared to coastal GECCO SSH in each region.

The conclusion to be reached from Figure 10 is that the large-scale coherent coastal sea level variability in GECCO is largely produced via net volume flow into and out of the western boundary region resulting in vertical divergence and a rise and fall of the mean surface height west of the 295°E meridian. This conclusion is supported by a correlation coefficient of 0.62 between $\langle \eta_{coast} \rangle$ and the time-integrated net volume flow across the 295°E meridian, which is significant at the 99% level.

5.3. Wind Forcing of the Basin-Scale Variability

The relationship between western North Atlantic sea level and atmospheric variability over the basin is a topic considered in previous studies. In particular, *Maul and Hanson* [1991] showed sea level in the SE and GOM regions was correlated significantly with the December to January SLP gradient between the Northeast and Southwest North Atlantic. The authors cite this gradient as a proxy for the North Atlantic Oscillation (NAO), but the NAO is generally defined as the meridional SLP gradient over the eastern North Atlantic. *Woolf et al.* [2003] compared the traditionally defined NAO with tide gauge sea levels along the Atlantic and GOM coasts of North America and found only a small correlation with sea level in the NE and little correlation with the SE and GOM regions. Calculations of the relationship between the NAO and western boundary sea level over the temporal span of our analysis support the conclusions of *Woolf et al.* [2003]. In addition, the wind field over the basin has been directly related to sea level in the basin interior [*Sturges and Hong*, 1995] and on the western boundary in the NE region [*Hong et al.*, 2000].

We are primarily interested in basin-scale variability, and thus we investigate the relationship between the basin-scale sea level coherence and the large-scale wind field via the Sverdrup relation, which describes the net movement of ocean volume in response to large-scale changes in wind forcing. The Sverdrup relation [*Sverdrup*, 1947] is the result of vertically integrating the linearized time-independent horizontal vorticity equation and is given by

$$V = \frac{\nabla_H \times \tau_w}{\rho \beta}, \tag{9}$$

where V is meridional volume transport in the interior, ∇_H is the horizontal gradient operator, τ_w is surface wind-stress, ρ is the density of sea water, and $\beta = df/dy$ is the meridional gradient of the Coriolis parameter.

Table 2. Statistics Relating the Diagnostic Terms and Model SSH at the Coast in Each Region[a]

Region	$\mathbf{r^2}(\eta_{coast}, \bar{\eta}+\eta_{tilt})$	$\mathbf{r^2}(\eta_{coast}, \bar{\eta})$	$\mathbf{r^2}(\eta_{coast}, \eta_{tilt})$	$\mathbf{r^2}(\bar{\eta}, \eta_{tilt})$
CS 1	**0.43**	**0.36**	0.23	**0.11**
CS 2	**0.47**	**0.76**	0.01	0.06
GOM	**0.65**	**0.89**	0.18	**0.14**
SE	**0.66**	**0.34**	0.11	0.16
NE	**0.69**	**0.23**	0.16	**0.30**

[a]Values significant at the 99% level are bold, where the number degrees of freedom are determined by the integral timescale of *Davis* [1976].

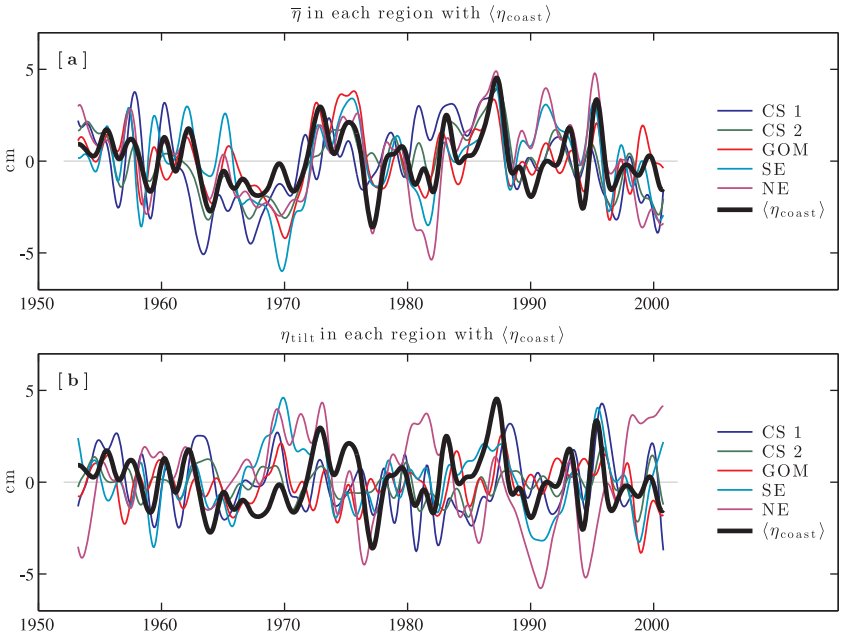

Figure 9. (a) Time series of $\bar{\eta}$ from each region (thin colored lines) with the average of the five regional coastal height curves from GECCO ($\langle\eta_{coast}\rangle$, thick black line). (b) Same as Figure 9a, but with time series of η_{tilt} from each region.

In order to conserve volume, the average meridional Sverdrup transport over some latitude range in the basin interior must be balanced by return flow in the boundary current. Thus, the average wind-stress-curl over some latitude range is expected to be related to volume transport in the boundary current and, by extension, η_{tilt}. We did not find η_{tilt} to be responsible for the basin-scale sea level coherence, and therefore we conclude that the average wind-stress-curl over the basin is not the driver of the large-scale variability.

An additional consideration, however, is the result of divergence in the Sverdrup transport. In other words, what is the effect of *dV/dy* on sea level in the western boundary? We showed in Figure 10 that the basin-scale coastal height variability on the western boundary in GECCO is largely accounted for by net vertically integrated zonal volume transport across the 295°E meridian. We now hypothesize that the net zonal transport across 295°E into the western boundary region may be due to convergence of the Sverdrup transport east of the meridian in the basin interior. To test this hypothesis, we time-integrated the difference between Sverdrup transport outside the boundary region in the north where 295°E intersects North America (~43° N) and in the south where 295°E intersects South America (~10° S). This is similar to equation (3), and can be written

$$\bar{\eta}_{Sv} = -\frac{1}{A}\int_{t_0}^{t}(V_N - V_S)dt, \tag{10}$$

where $V_N(V_S)$ is the Sverdrup transport between 295°E and the eastern boundary at the latitude where 295°E intersects North (South) America. In practice, the wind-stress-curl at each latitude was calculated as a line integral around a 3° band centered on the latitude in question.

Table 3. Statistics Relating the Diagnostic Terms and the Mean of the Five Regional Coastal Height Curves $\langle\eta_{coast}\rangle$[a]

Region	$r^2(\langle\eta_{coast}\rangle, \bar{\eta})$	$r^2(\langle\eta_{coast}\rangle, \eta_{tilt})$
CS 1	**0.30**	0.03
CS 2	**0.41**	0.01
GOM	**0.47**	0.02
SE	**0.32**	0.10
NE	**0.50**	0.01

[a]Values significant at the 99% level are bold, where the number degrees of freedom are determined by the integral timescale of *Davis* [1976].

The result of this calculation is shown in Figure 11 with the average SSH in the western boundary region. The correlation between the two curves is 0.68, and it is significant at the 99% level. It is apparent that the two curves agree better at lower frequencies, which is expected since the Sverdrup relation is time-independent. The assumption of time-independence is based on a time-scale long enough for the ocean to reach equilibrium with the wind-forcing, i.e., a time-

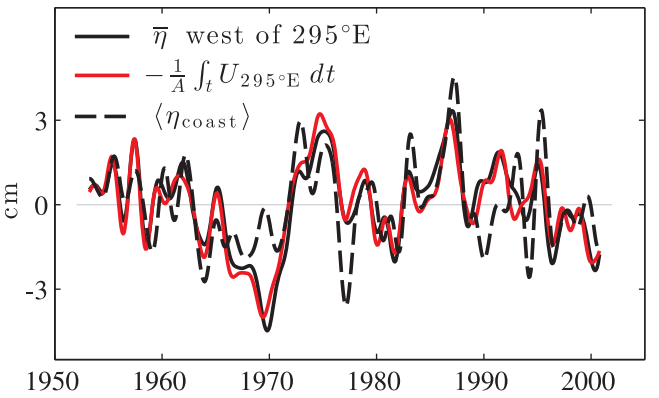

Figure 10. Average surface height west of the 295°E meridian from GECCO (black solid), time-integrated volume transport across the 295°E meridian scaled to sea surface height (red), and the average of the five regional coastal height curves (black dashed). The correlation between the solid black and red lines is 0.96. The correlation between the red and dashed black lines is 0.62. Both correlations are significant at the 99% level.

scale long enough for Rossby waves to reach the western boundary. Thus, the calculation is likely to perform better at decadal time-scales. Given the simplicity of the calculation, the significant correlation is convincing, and we conclude that the basin-scale coherence of sea level on the western North Atlantic boundary is primarily due to divergence of the Sverdrup transport in the basin interior east of the 295°E meridian resulting in a net zonal flow across the meridian.

Due to the linearity of the integration in (10), we can also differentiate between the contributions to the integral from the southern and northern edges of the domain,

$$\bar{\eta}_{Sv} = -\frac{1}{A}\int_{t_0}^{t} V_N dt + \frac{1}{A}\int_{t_0}^{t} V_S dt = \bar{\eta}_{Sv,N} + \bar{\eta}_{Sv,S}. \quad (11)$$

The individual contributions from the north and south are shown in Figure 11 as the thin solid and dashed lines. It is apparent from the two curves that a majority of the variability in the Sverdrup divergence calculation is due to variability in the Sverdrup transport in the north. In fact, the correlation between the average SSH in the western boundary region and only the first term on the right-hand side of (11) is 0.63.

6. Summary and Discussion

Coastal sea level variations at interannual and longer periods on the western boundary of the North Atlantic have been shown to be coherent over various regions of the western boundary coastline [e.g., *Thompson*, 1986; *Maul and Hanson*, 1991; *Häkkinen*, 2000; *Douglas*, 2005]. We show that this coherence extends along the entire length of the western boundary from Nova Scotia to the Caribbean, and the purpose of this analysis was to understand the physical mechanisms responsible for this basin-scale coherence. In order to simplify the analysis, we first averaged covarying tide gauge sea level records into four regional curves. These four curves account for almost 80% of the variance in the low-passed sea level data set in Table 1. Oceanographic data, however, is insufficient to differentiate between mechanisms of variability over the time period of interest. Thus, we used output from an ocean model to diagnose the role of leading order processes in the observed variability.

The observed regional variability from tide gauges is reproduced in the SSH fields of the GECCO model to good approximation, and in particular, there is a component of coastal western North Atlantic SSH in GECCO that is coherent between all regions. We formulated a simple diagnostic to investigate the mechanism(s) responsible for the coherence and applied it to the model output. A key difference between the formulation of our analysis and that of previous studies is how zonal transport into the western boundary region is allowed to affect sea level at the coast. We elected to retain vertical divergence in the continuity equation despite large horizontal velocities in the western boundary region, because the rates of sea level change in question are not small compared to the vertical velocities. As a result, our analysis allowed for geostrophic tilting of the surface due to meridional divergence as in *Hong et al.* [2000], but also for a uniform rise and fall of the surface due to vertical divergence.

We find that both processes can be important in any particular region, but it is the uniform rise and fall in each region that is responsible for the basin-scale, low-frequency coherence between regions. Furthermore, the variability of the average surface height in each region is highly correlated with the time-integrated

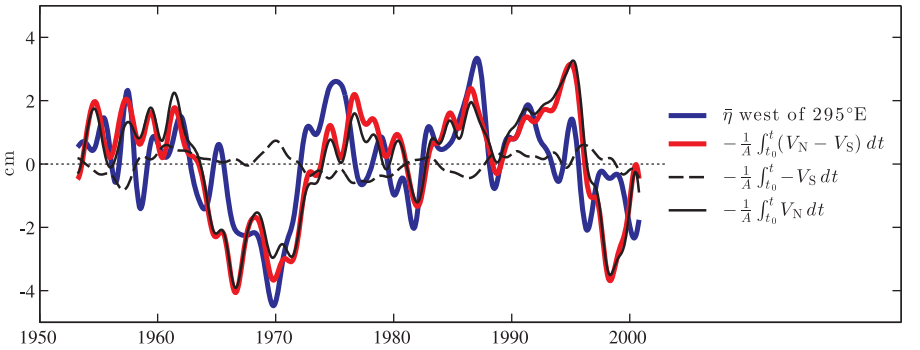

Figure 11. Average GECCO SSH west of the 295°E meridian ($\bar{\eta}$, blue) with time-integrated net Sverdrup transport in the basin interior (red). The correlation between the blue and red curves is 0.68.

zonal volume transport across the 295°E meridian. This suggests the basin-scale coherence of coastal SSH in GECCO is due to basin-scale, zonal redistributions of volume into and out of the western boundary region. The zonal redistribution manifests as vertical divergence and a uniform rise and fall of the surface.

The net volume transport into the western boundary region was found to be related to divergence of Sverdrup transport in the basin interior, and variability of the divergence is dominated by variability at the northern extent of the domain. These results are consistent with one of the important conclusions of *Hong et al*. [2000], which is that including meridional variation in the wind-stress-curl field is essential in accounting for western boundary sea level variability. Our interpretation is that the meridional variation in wind-stress-curl gives rise to the Sverdrup divergence.

A final consideration is how *Hong et al*. [2000] were able to achieve high correlations in their analysis despite not including vertical divergence. We suggest three factors that may contribute to the discrepancy. First, the results of *Hong et al*. [2000] focused on coastal variability in the region we defined as the NE. Our analysis showed that the tilting term, which is analogous to the mechanism proposed by *Hong et al*. [2000], is most important in this region and as important as variability in the average height of the surface. Second, *Hong et al*. [2000] did allow the average height of the surface to change in the coastal region by changing the offshore boundary condition of their coastal model. Zonal transport into the region was balanced by acceleration of the boundary current and tilting of the surface, but the tilting was always relative to the offshore boundary condition. The boundary condition was a function of the wind-stress-curl over the basin as it was set by the solution of their Rossby wave model. Our results suggest that divergence in the Sverdrup transport gives rise to the vertical divergence in the boundary region, but given that the Sverdrup transport is also a function of the wind-stress-curl, it is possible the information in our Sverdrup calculations may be included in the analysis of *Hong et al*. [2000] via the offshore boundary condition. Finally, the filter applied by *Hong et al*. [2000] considerably reduced the number of degrees of freedom in their calculations compared to the filter used in our analysis. As a result of the filter and the length of the time series, the success of their methodology was predicated on reproducing a single large decadal event in the 1970s. Our filter retained more degrees of freedom, and thus our results are less likely to have occurred by chance.

Acknowledgments
We would like to thank Eric Firing for enlightening discussion and the suggestion to diagnose a model. We also thank Don Chambers for insight and assistance concerning calculations of the equilibrium pole tide. The tide gauge sea level data used in this study are available from the website of the Permanent Service for Mean Sea Level (www.psmsl.org), and output from the GECCO simulation can be downloaded from the Integrated Climate Data Center (www.icdc.zmaw.de).

References

Bingham, R. J., and C. W. Hughes (2009), Signature of the Atlantic meridional overturning circulation in sea level along the east coast of North America, *Geophys. Res. Lett.*, *36*, L02603, doi:10.1029/2008GL036215.

Cazenave, A., and R. S. Nerem (2004), Present-day sea level change: Observations and causes, *Rev. Geophys.*, *42*, RG3001, doi:10.1029/2003RG000139.

Chandler, S. C. (1891), On the variation of latitude, I, *Astron. J.*, *11*(248), 59–61.

Curry, R. G., and M. S. McCartney (2001), Ocean gyre circulation changes associated with the North Atlantic oscillation, *J. Phys. Oceanogr.*, *31*(12), 3374–3400.

Davis, R. E. (1976), Predictability of sea surface temperature and sea level pressure anomalies over the North Pacific ocean, *J. Phys. Oceanogr.*, *6*(3), 249–266, doi:10.1175/1520-0485(1976)006 <0249:POSSTA >2.0.CO;2.

Douglas, B. C. (2005), Gulf of Mexico and Atlantic coast sea level change, in Circulation in the Gulf of Mexico: Observations and Models, Geophys. Monongr. Ser., edited by W. Sturges and A. Lugo-Fernández, pp. 111–121, AGU, Washington, D. C.

Eden, C., and T. Jung (2001), North Atlantic interdecadal variability: Oceanic response to the North Atlantic oscillation (18651997), *J. Clim.*, *14*, 676–691.

Ezer, T., L. P. Atkinson, W. B. Corlett, and J. L. Blanco (2013), Gulf Stream's induced sea level rise and variability along the U.S. mid-Atlantic coast, *J. Geophys. Res. Oceans*, *118*, 685–697, doi:10.1002/jgrc.20091.

Häkkinen, S. (2000), Decadal AirSea interaction in the North Atlantic based on observations and modeling results, *J. Clim.*, *13*(6), 1195–1219, doi:10.1175/1520-0442(2000)013 <1195:DASIIT >2.0.CO;2.

Häkkinen, S. (2001), Variability in sea surface height: A qualitative measure for the meridional overturning in the North Atlantic, *J. Geophys. Res.*, *106*(C7), 13,837–13,848, doi:10.1029/1999JC000155.

Hong, B. G., A. J. Clarke, and W. Sturges (2000), Sea level on the US east coast: Decadal variability caused by open ocean wind-curl forcing, *J. Phys. Oceanogr.*, *30*(8), 2088–2098.

Kalnay, E., et al. (1996), The NCEP/NCAR 40-year reanalysis project, *Bull. Am. Meteorol. Soc.*, *77*(3), 437–471.

Köhl, A., and D. Stammer (2008), Decadal sea level changes in the 50-year GECCO ocean synthesis, *J. Clim.*, *21*(9), 1876–1890, doi:10.1175/2007JCLI2081.1.

Köhl, A., D. Dommenget, K. Ueyoshi, and D. Stammer (2006), The Global ECCO 1952 to 2001 Ocean Synthesis, Tech. Rep. 40, Consortium for Estimating the Climate and Circulation of the Ocean (ECCO), Institut für Meereskunde, Universität Hamburg, Hamburg, Germany.

Kolker, A. S., and S. Hameed (2007), Meteorologically driven trends in sea level rise, *Geophys. Res. Lett.*, *34*, L23616, doi:10.1029/2007GL031814.

Marshall, J., A. Adcroft, C. Hill, L. Perelman, and C. Heisey (1997a), A finite-volume, incompressible Navier Stokes model for studies of the ocean on parallel computers, *J. Geophys. Res.*, *102*(C3), 5753–5766, doi:10.1029/96JC02775.

Marshall, J., C. Hill, L. Perelman, and A. Adcroft (1997b), Hydrostatic, quasi-hydrostatic, and nonhydrostatic ocean modeling, *J. Geophys. Res.*, *102*(C3), 5733–5752, doi:10.1029/96JC02776.

Maul, G. A., and K. Hanson (1991), Interannaul coherence between North Atlantic atmospheric surface pressure and composite southern U.S.A sea level, *Geophys. Res. Lett.*, *18*(4), 653–656, doi:10.1029/91GL00141.

Maul, G. A., F. Chew, M. Bushnell, and D. A. Mayer (1985), Sea level variation as an indicator of Florida current volume transport: Comparisons with direct measurements, *Science*, *227*(4684), 304–307.

Miller, L., and B. C. Douglas (2007), Gyre-scale atmospheric pressure variations and their relation to 19th and 20th century sea level rise, *Geophys. Res. Lett.*, *34*, L16602, doi:10.1029/2007GL030862.

Miller, S. P., and C. Wunsch (1973), The pole tide, *Nature*, *246*, 98–102.

Montgomery, R. B. (1938), Fluctuations in monthly sea level on eastern US coast as related to dynamics of western North Atlantic ocean, *J. Mar. Res.*, *1*(2), 165–185.

Montgomery, R. B. (1941), Sea level difference between Key West and Miami, Florida, *J. Mar. Res.*, *4*(1), 32–37.

Sallenger, A. H., K. S. Doran, and P. A. Howd (2012), Hotspot of accelerated sea-level rise on the Atlantic coast of North America, *Nat. Clim. Change*, *2*(8), 1–5, doi:10.1038/nclimate1597.

Sturges, W., and B. G. Hong (1995), Wind forcing of the Atlantic thermocline along 32-degrees-N at low-frequencies, *J. Phys. Oceanogr.*, *25*(7), 1706–1715.

Sverdrup, H. U. (1947), Wind-driven currents in a Baroclinic ocean; with application to the equatorial currents of the Eastern Pacific, *Proc. Natl. Acad. Sci. U. S. A.*, *33*(11), 318–326, doi:10.1073/pnas.33.11.318.

Thompson, K. R. (1986), North Atlantic sea-level and circulation, *Geophys. J. Int.*, *87*(1), 15–32, doi:10.1111/j.1365-246X.1986.tb04543.x.

Vondrak, J., C. Ron, I. Pesek, and A. Cepek (1995), New global solution of Earth orientation parameters from optical astrometry in 1900–1990, *Astron. Astrophys.*, *297*, 899–906.

White, N. J., J. A. Church, T. Aarup, W. S. Wilson, P. L. Woodworth, C. M. Domingues, J. R. Hunter, and K. Lambeck (2008), Understanding global sea levels: Past, present and future, *Sustain. Sci.*, *3*(1), 9–22, doi:10.1007/s11625-008-0042-4.

Woolf, D. K., M. N. Tsimplis, and A. G. P. Shaw (2003), Influence of the North Atlantic oscillation on sea-level variability in the North Atlantic region, *Global Atmos. Ocean Syst.*, *9*(4), 145–167, doi:10.1080/10236730310001633803.

Wu, L., and Z. Liu (2005), North Atlantic decadal variability: AirSea coupling, oceanic memory, and potential northern hemisphere resonance, *J. Clim.*, *18*(2), 331–349, doi:10.1175/JCLI-3264.1.

Wunsch, C., D. V. Hansen, and B. D. Zetler (1969), Fluctuations of the Florida Current inferred from sea level records, *Deep Sea Res.*, *16*, 447–470.